THE ASTROPHYSICAL JOURNAL, 180:987–1010, 1973 March 15


# A MEASUREMENT OF COSMIC-RAY RIGIDITY SPECTRA ABOVE 5 GV/$c$ OF ELEMENTS FROM HYDROGEN TO IRON*

L. H. SMITH, A. BUFFINGTON, G. F. SMOOT, AND L. W. ALVAREZ
Space Sciences Laboratory, University of California, Berkeley
AND
M. A. WAHLIG
Lawrence Berkeley Laboratory, University of California, Berkeley
*Received 1972 July 24*

## ABSTRACT

This paper presents measurements of the differential rigidity spectra of primary cosmic-ray nuclei between 5 GV/$c$ and 100 GV/$c$. These measurements were performed with a balloon-borne superconducting magnetic spectrometer containing scintillation detectors, optical spark chambers, and associated electronics. We present a rigidity spectrum for each element from hydrogen through oxygen and for groups of elements through the iron group. In our data, at large rigidities, the elements lithium, beryllium, boron, and nitrogen become increasingly rare relative to the other elements. Since these four elements are thought to be fragmentation products from the interactions of carbon, oxygen, or heavier cosmic-ray elements with the interstellar gas, one possible explanation of this result is that less interstellar material was traversed by higher-rigidity nuclei in the cosmic rays.

*Subject headings:* abundances, cosmic-ray — cosmic rays

## I. INTRODUCTION

Recent years have seen an increasing interest in the measurement and interpretation of primary nuclear cosmic-ray fluxes. The comparison between the abundances of cosmic-ray nuclei and "universal abundances" has been interpreted as providing evidence that these cosmic-ray nuclei had their origin in hot evolved stellar environments (Clayton 1968). Currently, supernovae seem to be the best candidates for the source of nuclear cosmic rays, whether they were created and accelerated by a shock-wave mechanism (Colgate and White 1966) or by a rotating neutron-star remnant of the supernova blast (Gold 1968; Ostriker and Gunn 1969; Kulsrud, Ostriker, and Gunn 1971; Goldreich and Keeley 1969). The observed abundance of the "light" elements (Li, Be, B) relative to the "medium" elements (C, N, O) indicates that the cosmic rays have passed through 3–5 g cm$^{-2}$ of interstellar material on their way from the sources to detectors at Earth (Shapiro and Silberberg 1970). For a number of years the extreme isotropy of the cosmic rays seemed to require an extragalactic origin, or at least a metagalactic containment volume (Hayakawa 1969). Recently, however, E. N. Parker and others have convincingly reconciled the isotropy measurements with the view that the cosmic rays have originated mostly in our Galaxy and have been confined in their propagation to a volume not much larger than the galactic disk (Jokipii and Parker 1969; Lingenfelter 1969; Speller, Thambyahpillai, and Elliot 1972).

A study of the energy spectra of the nuclear cosmic rays provides information about the mechanisms for acceleration, interstellar propagation, and galactic containment.

* This work supported in full by NASA contract NAS 9-7801.

The distribution function of cosmic-ray matter path length is of particular interest. Early workers used a "slab" model in which all particles passed through the same amount of material. However, analysis of the spectra below 500 MeV per nucleon, where ionization losses have played a major role, indicates that an exponential distribution function seems to be a better choice (Shapiro and Silberberg 1970; Gloeckler and Jokipii 1970). Other workers have fitted the data with a two-component model (Comstock 1969). In either model the particles are thought to be contained and propagated in a diffusive interstellar medium, within a containment volume whose least dimension is probably the thickness of the galactic disk. This point of view is further supported by observations of the total cosmic radiation energy spectrum, which follows a power law up to about $10^6$ or $10^7$ GeV, then becomes abruptly steeper. The steepening can be attributed to a breakdown of the containment, because at $10^6$ GeV the radii of curvature of the particles in microgauss galactic magnetic fields are comparable to the size of the containment volume. Poorer containment leads to both smaller cosmic-ray fluxes and shorter mean lifetimes in the Galaxy. The constancy of the power-law behavior up to the break point at $10^6$ GeV suggests that the average amount of material traversed and the distribution function for path length remain approximately constant throughout the lower energy range. On the other hand, Cowsik (1970) has shown recently that if the sub-millimeter radiation of Shivanandan (Shivanandan, Houck, and Harwit 1968) is universal, the average amount of material traversed, and hence the ratio of light to medium nuclei in the cosmic rays, could be a rather strongly decreasing function of rigidity, even in the rigidity range 1–100 GV/$c$. Since most of the accurate measurements of the spectra of individual elements have been made for rigidities at or below a few GV/$c$, a limit imposed both by techniques and fluxes, it is certainly of interest to extend the measurements up in rigidity as far as possible.

The light-element spectra have also been analyzed for the elusive $^{10}$Be which could provide a radioactive dating of the cosmic rays. Most recent compilations still allow ages of cosmic-ray beryllium to range from $10^6$ to $10^8$ years (O'Dell *et al.* 1971). More $^{10}$Be should survive at high energies because of relativistic time dilation. The difference between complete decay and complete survival is estimated to cause a change in the ratio (Be/B) from 0.3 to 0.4. Analysis of the spectra of these elements over a wide range of energies with good statistics might finally give an unambiguous age determination.

In this paper we present the completed analysis of the rigidity spectra recorded in two balloon flights of a superconducting magnetic spectrometer apparatus. Preliminary results have already been presented in conferences (Buffington *et al.* 1971; Smoot *et al.* 1972*b*). The result of an antimatter search in these data has been published elsewhere (Buffington *et al.* 1972). The differential spectra presented here extend from 5 to 100 GV/$c$ in rigidity for individual elements from hydrogen through oxygen and for groups through iron. These high statistics measurements allow, for the first time, extension of detailed interpretation of cosmic-ray abundances into the rigidity range between 10 and 100 GV/$c$.

## II. EXPERIMENTAL APPARATUS

A complete description of the experimental apparatus is published elsewhere (Smith *et al.* 1972). Figure 1 shows the experimental configuration. A superconducting coil with its associated Dewar and liquid-helium reservoir is at the center of the apparatus. Once the current in the coil is made persistent, its magnetic field will remain as long as liquid helium is left in the Dewar, unless the persistency switch which completes the current loop is opened.

Optically viewed spark chambers located above and below the magnet mark the trajectory of the particle being analyzed. The three scintillation counters $S_1$, $S_2$, and

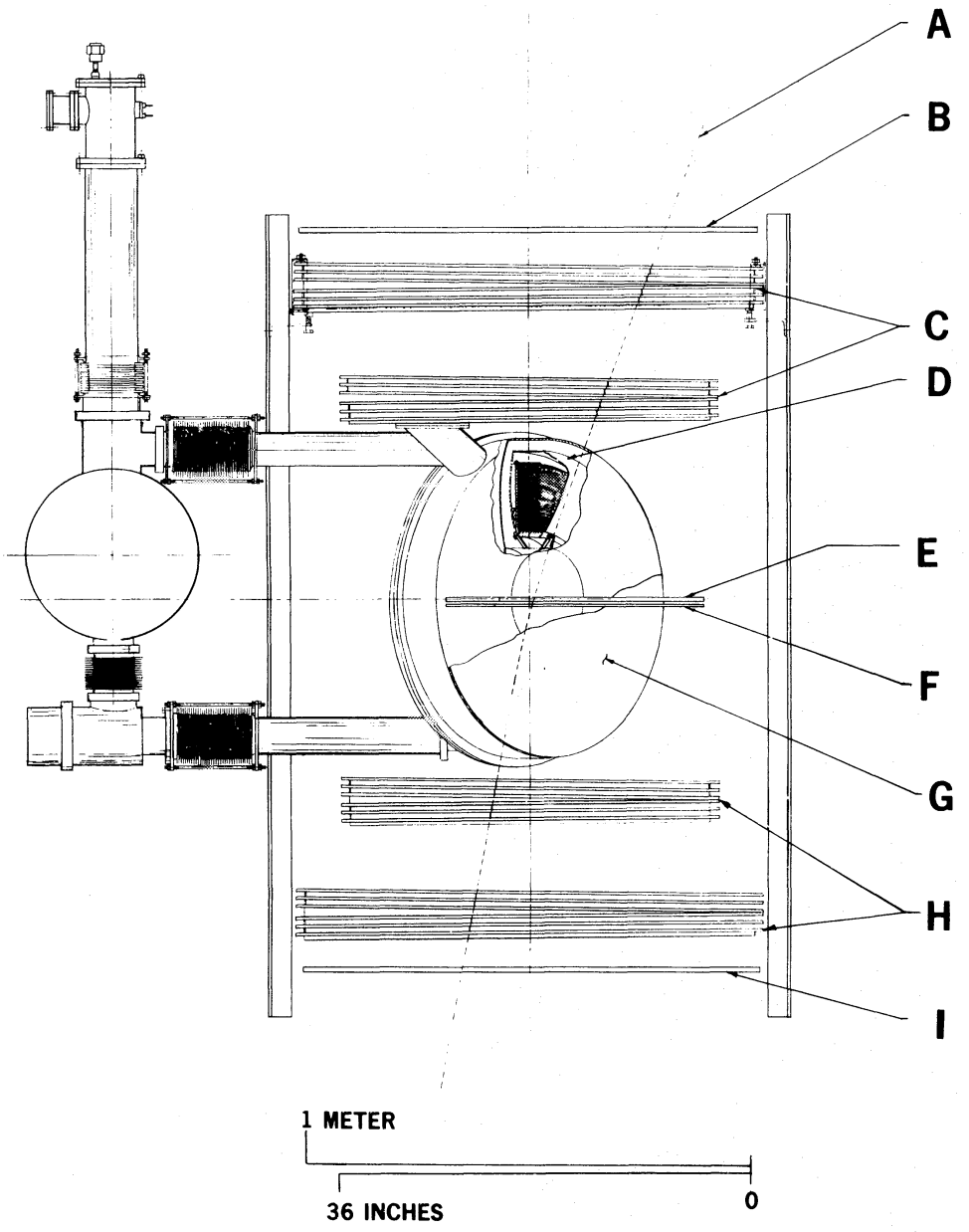


FIG. 1.—Schematic diagram of the apparatus. *A*, particle trajectory; *B*, $S_1$ trigger counter 100 × 100 cm, Pilot Y; *C*, spark chambers; *D*, superconducting magnet; *E*, CsI 18 × 50 cm both sides; *F*, $S_2$ trigger counter 18 × 50 cm both sides; *G*, anticoincidence counter 61 cm disk both sides; *H*, spark chambers; *I*, $S_3$ trigger counter 100 × 100 cm, Pilot Y.

$S_3$ define the geometry, measure the charge, and provide a trigger for the spark chambers. The $S_2$ scintillator consists of two identical halves, placed symmetrically on either side of the magnet. A pair of anticoincidence scintillators, one on each side of the magnet, can be made to reject the multiprong background events which result from hadron interactions in the magnet coil and the other surrounding material. Radio commands select the trigger thresholds in the counters $S_1$, $S_2$, and $S_3$, providing a choice of data taking on particles with charge $Z \geq 1$, $Z \geq 2$, $Z \geq 3$, or $Z \geq 4$. Radio control also provides for either inclusion or exclusion of the anticoincidence

scintillators in the spark-chamber trigger criterion. The geometry factor of the apparatus, for the case of the anticoincidence scintillators included, is 643 ± 8 cm$^2$ sterad. When the magnet is operated at its full current of 100 amperes, the $|\int \boldsymbol{B} \times d\boldsymbol{l}|$ for bending the particles varies from 3 to 10 kilogauss-meters depending on distance from the magnet, with a mean of 5 kilogauss-meters. The mean maximum detectable rigidity at 100 amps is 120 GV/$c$. However, for flight data taken at reduced magnet current and with our automatic film measurements, the mean maximum detectable rigidity was reduced to 50 GV/$c$.

Either or both of two 35-mm cameras can record both 90° stereo views of the sparks, along with an extensive array of fiducial lights, a clock, and a data-box panel of lights for binary data readout. Operation of the cameras requires a dead time of 0$^s$.218 for each event recorded. The film capacity of the cameras is 60,000 frames for a single flight. A calibration sequence initiated frequently during data taking provides a check on possible changes in the spark chamber optical system. The spatial resolution of the spark chamber optics was ±0.14 mm.

The pulse heights from plastic scintillators $S_1$ and $S_3$, and from cesium iodide scintillators just above the $S_2$ counters, are digitized and presented on the data box. pulse heights from both the anode and a dynode of each photomultiplier system are recorded. Analysis of these pulse heights yields a charge determination with a half-width at half-maximum of about 0.2 charge for elements through oxygen.

## III. DATA TAKING

The data were accumulated during two balloon flights of the magnetic spectrometer from Palestine, Texas. The first flight was made on the evening of 1970 September 18, and the gondola floated at 4.8 g cm$^{-2}$ residual atmosphere for approximately 6 hours of magnet-on data taking. The second flight began on the evening of 1971 May 7, and the gondola floated at 5.9 g cm$^{-2}$ for approximately 13 hours of magnet-on data taking. There were three differences in the apparatus between the flights. On the first flight, the magnet was made persistent at 70 A, compared to a persistent current of 80 A for the second flight. Increased liquid-helium reservoir capacity for the second flight allowed 20 hours of magnet operation on a filling of liquid helium, an increase of 10 hours. Finally, the cesium iodide scintillator was eliminated from the spectrometer for the second flight to reduce the detector material from[1] 6.0 g cm$^{-2}$ to 4.0 g cm$^{-2}$; the $S_2$ scintillator (Pilot B) was pulse-height analyzed in place of the cesium iodide.

TABLE 1

DATA-TAKING MODES DURING THE FLIGHTS

| Flight | Data Mode | Anti–Detector | Real Time (seconds) | Exposure Live Time (seconds) | Pictures Taken | Good Events Obtained |
|---|---|---|---|---|---|---|
| 1970 September..... | $Z \geq 1$ | IN | 1771 | 99 | 6384 | 2423 |
| | $Z \geq 2$ | IN | 6440 | 1635 | 18,413 | 5926 |
| | $Z \geq 3$ | IN | 11,551 | 9747 | 5261 | 2500 |
| | $Z \geq 3$ | OUT | 1811 | 885 | 3698 | 295 |
| 1971 May..... | $Z \geq 2$ | IN | 3480 | 838 | 10,351 | 3983 |
| | $Z \geq 3$ | IN | 10,440 | 8744 | 6219 | 2886 |
| | $Z \geq 3$ | OUT | 2160 | 954 | 4654 | 410 |
| | $Z \geq 4$ | OUT | 23,640 | 16,741 | 26,865 | 6971 |

[1] This value, reduced from the 6.9 g cm$^{-2}$ reported in Smith *et al.* (1972), represents the result of a more accurate measurement of the spark-chamber plate grams cm$^{-2}$.

Table 1 shows the data-taking modes during the flights. The term "data mode" refers to the minimum charge of an accepted particle as set by the scintillator pulse-height threshold for spark-chamber trigger. The next column indicates whether the anticoincidence detector was used in the spark-chamber trigger criterion. The actual exposure live time was obtained from the "real time" data period by subtracting the off-time for camera winding and calibration sequences.

The final column of table 1 indicates the number of events finally passing the data analysis criteria to be described in the next section. In addition to the data taking shown in the table, approximately 20,000 pictures were obtained on the first flight and 10,000 on the second flight after the magnet was de-energized. These "straight tracks" were used to correct for small uncertainties in alignment between the spark chambers.

## IV. DATA ANALYSIS

The data analysis procedure efficiently selected the legitimate events from among the pictures. It then calculated the indicated charge and rigidity for each event. Because this is the first experiment of its kind, an understanding of our techniques is required for critical evaluation of our data. We will therefore present a fairly detailed description of the data analysis.

### *a) Scanning Classifications and Background*

A scan of flight data taken with the anticoincidence detector included in the spark-chamber trigger criterion (anti-IN) showed that about 50 percent of the pictures were multiple-track events, roughly independent of the threshold selection for the trigger counters. For the data taken in the mode charge $Z \geq 3$, anti-OUT, however, this background increased to about 85 percent. The background for each data-taking mode is consistent with that expected from secondary particles (mostly produced by hadron interactions in the material of our gondola) operating the trigger counters. Many of the background events had several prongs in the spark chambers which converged toward various objects, such as the magnet coil or the top shell of the gondola.

Another source of background was the fragmentation of heavy nuclei which interacted while passing through our equipment. This source of background is essentially unremovable. Highly charged nuclei also interacted electromagnetically with the material of the detectors, creating numerous delta-rays. In our spark chambers, however, the dense trail of ionization left by the primary particle robbed the spark energy from the delta-ray tracks, so the latter registered on the film only occasionally.

In order to separate the good from the background events, our scanners examined all of the magnet-on pictures taken during the flights. They classified each event as "good" if it had only a single track through all four spark chambers, sometimes accompanied by an extra track (presumably a delta-ray) showing in one or two chambers. All other events were classified as "failures" and were attributed to the background trigger processes mentioned above. Double scanning and other cross-checks indicated at 99 percent efficiency for the selection of ultimately good data by only a single pass with this scanning procedure.

### *b) Measuring and Fitting: Rigidity Determination*

All events were encoded on magnetic tape by the Lawrence Berkeley Laboratory's SASS machine, a computer-controlled cathode-ray tube encoder (Zurlinden 1967). The encoded events were filtered by a simple computer program which eliminated single spurious sparks judged not to be correlated with the main tracks. At this point

about half of the events labeled "good" by the scanners had the immediately acceptable topology of one track per chamber. The remainder were mostly events with associated delta-rays for which spark robbing was not complete. These were subjected to further processing by an interactive computer technique. The computer displayed on a cathode-ray tube all of the spark measurements to a scanner, who then deleted the spurious tracks. The result of this processing was that 98 percent of the events identified as "good" events did indeed have acceptable topologies.

The events selected and measured by the above procedure then had their spark coordinates reconstructed from the film plane into real space. The four sparks at each chamber level were averaged together for each event. These real-space coordinates were iteratively fitted with an allowed trajectory through the inhomogenous magnetic field using a least-squares technique. The parameters of this trajectory afforded a calculation of a rigidity value. The rms deviation served as a goodness-of-fit evaluation. Events were discarded which passed through the material of the magnet Dewar, which had a goodness-of-fit evaluation greater than four times the typical value, or finally which had a rigidity value well below geomagnetic cutoff ($\leq 3$ GV/$c$). Imposition of these criteria fixed the geometry of the apparatus (important only for anti-OUT data), eliminated multiprong background events which managed to meet the scanner's "good" topology requirement, and removed low-momentum atmospherically generated events. The low-momentum events were a considerable portion of the data for the $Z \geq 1$ and $Z \geq 2$ trigger modes (15 percent and 20 percent, respectively); for the $Z \geq 3$ and $Z \geq 4$ trigger modes they were negligible. The low-momentum events in the case of the $Z \geq 2$ trigger mode were caused by protons whose enhanced energy loss in the scintillators enabled them to meet the trigger threshold. Considering losses due to scanning, topological selection, and goodness-of-fit criterion, the total efficiency of the data analysis procedure was 97 percent. This figure indicates the percentage of good events which were ultimately used for charge determination.

### *c) Charge Determination*

Analysis of the pulse heights from the scintillators provided the charge distribution for the data. The apparent pulse height for each counter was corrected for zero-point drift in the electronics using the known gain difference between photomultiplier anode and dynode. The spark-chamber information was used to correct for spatial and angular variation in pulse-height response of the counters. Kinematic variation in light response of the scintillators was unimportant in our rigidity range.

The pulse-height distribution for each counter was made linear by placing the peaks for distinctive elements (helium, oxygen, silicon, and iron) at their appropriate charges. Known electronics nonlinearity and the $Z^2$ response of the scintillators provided an adequate explanation of the pulse height distribution peak locations for Pilot Y. No saturation was apparent in the Pilot Y scintillator even for incident iron nuclei. However, the saturation measured for Pilot B caused a 15 percent reduction of pulse height at silicon.

To assign a specific integer charge value for each event, we formed a three-dimensional scatter plot using the measured charge values from our three scintillators. An event had its charge fixed if it lay within a sphere of radius $\frac{1}{2}\sqrt{3}$ charges centered at the appropriate diagonal location for the element being considered. For the second flight, 84 percent of the elements met this selection criterion. Unfortunately, for the first flight, one of the cesium iodide scintillators suffered degraded performance (because of packing-oil leakage) and was essentially useless for charge determinations.

In order to give charge assignments to the events unable to meet the three-counter criterion above, we also considered two-dimensional scatter plots using any two of the three scintillators. Here, an event had its charge fixed if it lay within a circle of radius

$\frac{1}{2}\sqrt{2}$ charges, again centered at the appropriate diagonal location for the element being considered. Combining charge determinations from these two techniques we were able to assign charge to 98 percent of the events in the second flight and 93 percent of the events in the first flight. The 2 percent remaining for the second flight had greatly differing pulse heights and therefore appeared to be the last residues of multiprong background, or fragmenting nuclei. In order to display our charge resolution we averaged the two or three pulse heights which determined the integer charge value for each event. Figure 2 shows the resulting "average" charge values so measured for two portions of our data. The average charge was found to be independent of rigidity for each element. The charge resolution was about $\pm 0.2$ charges.

The data having charges assigned still contained a contamination of events in which nuclei had fragmented during their passage through the instrument. Frequently these events had both a good fit in the spectrometer and agreement among two of the three pulse-height measurements. Events with fragmentation were characterized by a smaller pulse height in the lower detectors. Examination of the 14 percent of the good data in which only two of the three scintillators agreed showed that 5 percent were fragmentation events, approximately one-half of the calculated expected number of fragmentations in the gondola material. The other half presumably failed the preceding data analysis criteria. Half of the 5 percent had their charge properly determined by the first two scintillators before they fragmented. Since the rigidity spectra of these fragmentation products were very similar to those of the parent elements, we are confident that there is no distortion of the rigidity spectra owing to the inclusion of this $2\frac{1}{2}$ percent background.

For elements with charges below fluorine, we were able to achieve essentially unambiguous identification of charge for each event. We estimate, using our scatter plot distributions, that an error in assigning charge occurred in about 2 percent of the events. However, for elements with charges greater than oxygen our charge resolution became worse. Three effects contributed to this degradation: (1) uncertainty in the spatial corrections, (2) small variations ($\sim 2$ percent) in photomultiplier gain as the data-taking progressed, and (3) inability to correct the electronic zero-point drift by anode and dynode comparison, since these elements were "on-scale" only for the dynode pulse height analysis. As a result, unambiguous charge assignment for each element was no longer possible above oxygen. For this reason, in presenting our rigidity spectra, we have placed the events above oxygen in groups.

## V. RELATIVE ABUNDANCES AND SYSTEMATIC ERRORS

A potential source of systematic error in calculating the relative abundances of the elements is the "spillover" from plentiful elements to their nearby rare neighbors, due to inadequate resolution. Lithium and fluorine are rare elements for which this source of error is at its extreme. Spillover events tend to cluster toward the plentiful element that was their source, so the charge distribution of a contaminated element has an anomalous appearance. Inspection of our data showed that lithium contained negligible spillover from helium, but that the odd-$Z$ elements above oxygen were contaminated. We have corrected our relative abundance table with our estimate of the incorrectly assigned events, which amounts to about 20 percent of the fluorine and 10 percent of the sodium and aluminum. The assigned errors in relative abundance for the very high $Z$ elements are therefore somewhat larger than the normal statistical errors because they include estimates of the systematic error in our technique. Table 2 shows the events of our flights grouped by charge.

We must correct the anti-IN data of table 2 to compensate for loss of good events due to delta-rays operating the anticoincidence scintillator. The probability of this occurring was an increasing function of charge and rigidity. A Monte Carlo calculation

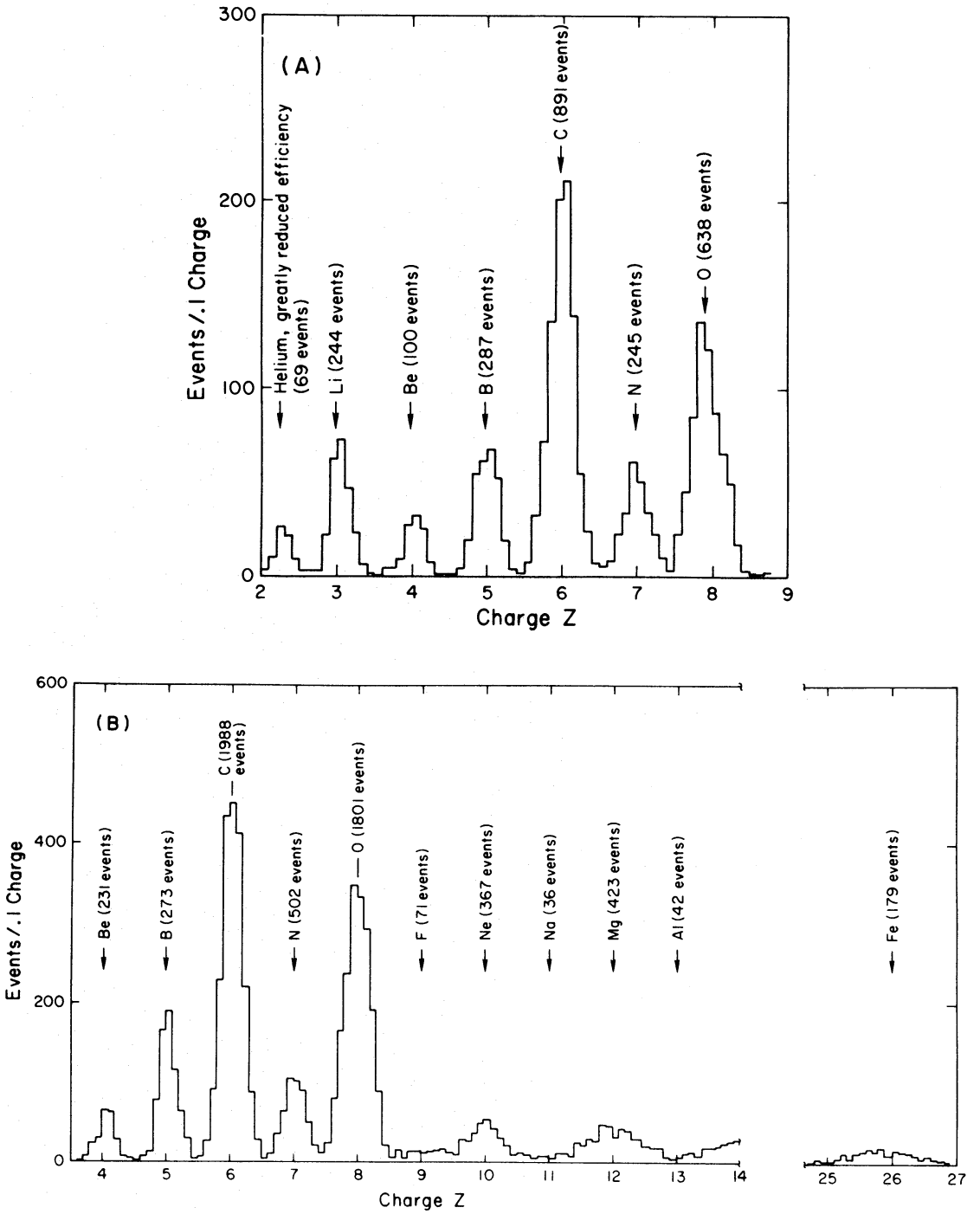


FIG. 2.—Charge distributions for two data samples: (*a*) Data mode $Z \geq 3$, anti-IN; (*b*) Data mode $Z \geq 4$, anti-OUT.

TABLE 2

OBSERVED EVENTS GROUPED BY CHARGE

| TRIGGER MODE | | $Z$ | | | | | | | | | | | | | | | |
|---|---|---|---|---|---|---|---|---|---|---|---|---|---|---|---|---|---|
| Threshold | Anti- | 1* (H) | 2* (He) | 3 (Li) | 4 (Be) | 5 (B) | 6 (C) | 7 (N) | 8 (O) | 9 (F) | 10 (Ne) | 11 (Na) | 12 (Mg) | 13 (Al) | 14 (Si) | 15–24 (P–Cr) | 25–28 (Fe Group) |
| **Flight 1** | | | | | | | | | | | | | | | | | |
| $Z \geq 1$ | IN | (2055) | 344 | 3 | 5 | 5 | 5 | 0 | 2 | ... | ... | ... | ... | ... | ... | ... | ... |
| $Z \geq 2$ | IN | ... | (5358) | 55 | 26 | 51 | 123 | 49 | 114 | ... | ... | ... | ... | ... | ... | ... | ... |
| $Z \geq 3$ | IN | ... | ... | 160 | 104 | 245 | 792 | 242 | 624 | ... | ... | ... | ... | ... | ... | ... | ... |
| $Z \geq 3$ | OUT | ... | ... | 18 | 12 | 18 | 85 | 25 | 62 | 2 | 10 | 0 | 27 | 3 | 18 | 11 | 4 |
| **Flight 2** | | | | | | | | | | | | | | | | | |
| $Z \geq 2$ | IN | ... | (3634) | 33 | 21 | 34 | 99 | 31 | 80 | ... | ... | ... | ... | ... | ... | ... | ... |
| $Z \geq 3$ | IN | ... | ... | 244 | 100 | 287 | 891 | 245 | 638 | ... | ... | ... | ... | ... | ... | ... | ... |
| $Z \geq 3$ | OUT | ... | ... | 25 | 16 | 43 | 108 | 23 | 104 | 8 | 13 | 1 | 24 | 1 | 18 | 16 | 10 |
| $Z \geq 4$ | OUT | ... | ... | ... | 231 | 673 | 1988 | 502 | 1801 | 71 ±10 | 367 | 36 ±7 | 423 | 42 ±8 | 337 | 321 | 179 |

* Due to trigger discrimination threshold, the data in parentheses are low: protons had an efficiency of 0.81 ± 0.10; helium, flight 1, had an efficiency of 0.87 ± 0.04; helium, flight 2, had an efficiency of 0.86 ± 0.05.

of this phenomenon predicted an average loss of about 15 percent of our carbon events, and 25 percent of our oxygen events. Oxygen varied from 25 percent to 35 percent loss as its rigidity increased from 10 GV/$c$ to 100 GV/$c$. We were able to verify these predictions in detail because a large portion of our data was taken with anti-OUT but with a light photographed with the sparks to indicate when a particle associated with the event had struck the anti. We found our predictions to agree with the data within 2 percent. After applying to the anti-IN data the charge- and rigidity-dependent correction indicated by the calculations, all difference between it and the anti-OUT data disappeared. The anti-IN data were not considered for charges above oxygen, however, because the size of the correction was uncomfortably large.

Table 2 was also modified for interaction losses in the gondola material. The losses which would be calculated directly from the amount of material in the gondola overestimate the actual losses because half of the fragmenting events are still included in table 2. The attenuation mean free paths used were taken from Cleghorn, Freier, and Waddington (1968), assuming the detector material had an average composition equivalent to air. Systematic errors introduced into the relative abundances by uncertainties in the effective attenuation grams $cm^{-2}$ and in the mean free paths are estimated to be of the order of 1 percent.

Table 3A presents the resulting relative abundances, normalized to carbon and corrected to the top of the spark chambers. The various data blocks from each flight were combined using the exposure live times from table 1.

Table 3B presents the relative abundances corrected to the top of the atmosphere. The residual grams include the gondola shell (0.5 g $cm^{-2}$) and, in the case of the second flight, the top scintillator (1 g $cm^{-2}$), as well as the actual residual atmosphere. Table 4 presents the fragmentation parameters used (Cleghorn *et al.* 1968; Silberberg and Tsao 1971; private communication with R. Silberberg). The final error estimates in table 3B do not include any increase to account for error in table 4, even though we feel that the corrections are quite uncertain. Correction to the top of the atmosphere does not greatly affect the data for the plentiful elements such as carbon and oxygen, but it is very important for beryllium and the rare odd-$Z$ elements above oxygen. For example, if the fragmentation parameter for producing beryllium from carbon were 0.04 instead of the 0.06 in table 4, the corrected beryllium abundance at the top of the atmosphere would be 4.6 percent instead of the 4.1 percent of table 3, for Flight 2 data.

Table 5 compares the combined data from both flights with some representative equivalent flights of other experimenters (Von Rosenvinge, Webber, and Ormes 1969*a*; Webber, Damle, and Kish 1972; Cassé *et al.* 1971*a*, 1971*b*). Qualitatively, our results are in agreement with the earlier measurements. On close inspection, however, there are greater differences between the experimental results than the statistical errors would permit. For example, our measurements of the light elements agree with those of Von Rosenvinge and of Cassé, but disagree with those of Webber. Also, disagreements occur for some of the elements above oxygen. It is not our purpose here to make a critique of other experiments. It is worthwhile, however, to discuss some of the potential sources of systematic, nonstatistical error in background rejection and charge selection which we have encountered in the design and in the data analysis of our experiment.

For incident charge below carbon, multiprong interaction backgrounds play an important role. Our anticoincidence scintillator and optical spark chambers with their visual rejection of multiprongs reduced this background to a few percent. Finally, our detailed trajectory-fitting through the magnetic field essentially eliminated the remainder of this background, even for the difficult element lithium, with its original multiprong background of nearly 100 times the signal. To minimize systematic errors, pulse-height information was considered only after the multiprong background had

TABLE 3

RELATIVE ABUNDANCE OF THE ELEMENTS, NORMALIZED TO CARBON

| Flight | Residual Atmosphere and Gondola Equivalent [g cm$^{-2}$] | Nominal Vertical Geomagnetic Cutoff [GV/$c$] | H | He | Li | Be | B | C | N | O | F | Ne | Na | Mg | Al | Si | P–Cr | Fe Group |
|---|---|---|---|---|---|---|---|---|---|---|---|---|---|---|---|---|---|---|
| **Part A** | | | | | | | | | | | | | | | | | | |
| 1.... | 5.4 | 4.35±0.14 | 26,000 ±2600 | 4050 ±200 | 21.4 ±1.4 | 13.6 ±1.1 | 31.7 ±1.8 | 100 ±3.2 | 32.3 ±1.9 | 89.1 ±3.5 | ... | ... | ... | ... | ... | ... | ... | ... |
| 2.... | 7.4 | 4.55±0.14 | ... | 4300 ±100 | 25.1 ±1.4 | 11.5 ±0.6 | 33.0 ±1.0 | 100 ±1.8 | 26.6 ±0.9 | 88.3 ±1.7 | 3.7 ±0.5 | 18.1 ±0.9 | 1.8 ±0.3 | 21.4 ±1.0 | 2.1 ±0.4 | 17.0 ±0.9 | 16.3 ±0.9 | 9.3 ±0.7 |
| **Part B** | | | | | | | | | | | | | | | | | | |
| 1.... | 0 | 4.35±0.14 | 24,000 ±2800 | 4000 ±180 | 16.4 ±1.7 | 8.4 ±1.4 | 25.1 ±2.2 | 100 ±3.9 | 31.4 ±2.3 | 93.1 ±4.4 | ... | ... | ... | ... | ... | ... | ... | ... |
| 2.... | 0 | 4.55±0.14 | ... | 4200 ±100 | 18.1 ±1.8 | 4.2 ±0.8 | 23.5 ±1.3 | 100 ±2.4 | 24.8 ±1.3 | 94.0 ±2.3 | 2.1 ±0.7 | 18.9 ±1.3 | 0.8 ±0.5 | 23.6 ±1.4 | 1.8 ±0.5 | 19.6 ±1.3 | 18.1 ±1.4 | 12.0 ±1.1 |

NOTE.—Part A corrected to top of the spark chambers; part B corrected to top of the atmosphere.

1973ApJ...180..987S

TABLE 4

MEAN FREE PATHS AND FRAGMENTATION PROBABILITIES USED FOR ATMOSPHERIC ATTENUATION AND CONTAMINATION

| Element | H | He | Li | Be | B | C | N | O | Ne | Mg | Si | P–Cr | Iron Group |
|---|---|---|---|---|---|---|---|---|---|---|---|---|---|
| Mean free path [g cm$^{-2}$] | 65.0 | 40.0 | 34.5 | 32.0 | 30.0 | 28.0 | 26.5 | 25.3 | 23.7 | 22.0 | 21.0 | 18.0 | 16.0 |
| Daughter: | Fragmentation Parameters | | | | | | | | | | | | |
| Lithium | ... | ... | ... | ... | 0.10 | 0.07 | 0.06 | 0.04 | 0.08 | 0.07 | 0.06 | ... | 0.14 |
| Beryllium | ... | ... | ... | ... | 0.16 | 0.06 | 0.05 | 0.08 | 0.07 | 0.03 | 0.05 | ... | 0.04 |
| Boron | ... | ... | ... | ... | ... | 0.17 | 0.08 | 0.07 | 0.10 | 0.05 | 0.06 | ... | 0.06 |
| Carbon | ... | ... | ... | ... | ... | 0.07 | 0.12 | 0.09 | 0.09 | 0.06 | 0.04 | ... | 0.04 |
| Nitrogen | ... | ... | ... | ... | ... | ... | 0.03 | 0.07 | 0.07 | 0.04 | 0.03 | ... | 0.02 |
| Oxygen | ... | ... | ... | ... | ... | ... | ... | 0.07 | 0.10 | 0.08 | 0.06 | ... | 0.04 |
| Fluorine | ... | ... | ... | ... | ... | ... | ... | ... | 0.09 | 0.07 | 0.05 | ... | 0.02 |
| Neon | ... | ... | ... | ... | ... | ... | ... | ... | 0.04 | 0.06 | 0.05 | ... | 0.01 |
| Sodium | ... | ... | ... | ... | ... | ... | ... | ... | ... | 0.06 | 0.05 | ... | 0.01 |
| Magnesium | ... | ... | ... | ... | ... | ... | ... | ... | ... | 0.04 | 0.07 | ... | 0.01 |
| Aluminum | ... | ... | ... | ... | ... | ... | ... | ... | ... | ... | 0.05 | ... | 0.01 |
| Silicon | ... | ... | ... | ... | ... | ... | ... | ... | ... | ... | 0.04 | ... | 0.01 |
| Phosphorus through chromium | ... | ... | ... | ... | ... | ... | ... | ... | ... | ... | ... | ... | 0.25 |
| Iron group | ... | ... | ... | ... | ... | ... | ... | ... | ... | ... | ... | ... | 0.17 |

TABLE 5

RELATIVE ABUNDANCE OF THE ELEMENTS ABOVE HELIUM NORMALIZED TO CARBON, BEFORE CORRECTION TO TOP OF ATMOSPHERE*

| | Von Rosenvinge *et al.* (1969*a*) | Webber *et al.* (1972) | Cassé *et al.* (1971) | This Experiment |
|---|---|---|---|---|
| Residual Atmosphere | 5.0–6.2 | 2.2 | 3.5–5.5 | ~6.5 |
| Material in Apparatus (perpendicular incidence) [g cm$^{-2}$]† | $\gtrsim$2.1 | 5.7 | 7.0 | 1.5 |
| Rigidity range [GV/*c*] | $\gtrsim$4 | >1.7 | >3.6 | $\gtrsim$4 |
| Flight dates | Spring 1967 | Summer 1970 | Summer–Fall 1969 | Fall 1970, Spring 1971 |
| Element | | | | |
| Lithium | 22 ± 1.6 | 17 ± 0.6 | ... | 23.0 ± 1.2 |
| Beryllium | 13.5 ± 1.3 | 9 ± 0.5 | 16 ± 2 | 12.4 ± 0.6 |
| Boron | 32 ± 2 | 29 ± 0.8 | 29 ± 1 | 32.5 ± 0.9 |
| Carbon‡ | 100 ± 4 | 100 ± 1.5 | 100 ± 7 | 100 ± 1.7 |
| Nitrogen | 24 ± 1.7 | 26 ± 0.7 | 26 ± 1 | 29.0 ± 0.8 |
| Oxygen | 87 ± 3.2 | 85 ± 1.3 | 93 ± 2 | 88.7 ± 1.5 |
| Fluorine | ... | 1.2 ± 0.1 | 3 ± 0.5 | 3.7 ± 0.5 |
| Neon | ... | 14 ± 0.6 | 15 ± 1 | 18.1 ± 0.9 |
| Sodium | ... | 2.5 ± 0.2 | 5 ± 0.7 | 1.8 ± 0.3 |
| Magnesium | ... | 17 ± 0.6 | 20 ± 2 | 21.4 ± 1.0 |
| Aluminum | ... | 2 ± 0.2 | 6 ± 1 | 2.1 ± 0.4 |
| Silicon | ... | 11 ± 0.5 | 16 ± 2 | 17.0 ± 0.9 |
| Phosphorus through Chromium | ... | 11 ± 0.5 | ... | 16.3 ± 0.9 |
| Iron group | ... | 9 ± 0.5 | ... | 9.3 ± 0.7 |

* Errors are statistical only.

† We have attempted for the other experiments to distinguish between grams cm$^{-2}$ which merely attenuate ("Apparatus") and which both attenuate and feed down as fragments ("Atmosphere").

‡ For comparisons between different experiments, the error in the determination of the abundance of carbon (defined to be 100 percent for each experiment) should be folded into the error for the element being compared. However, for the comparison of the abundances of two elements within a single experiment, only the errors for those two elements are relevant.

been eliminated. Further, the resulting pulse-height distributions showed none of the characteristics of the pulse-height distribution for the multiprong background, thereby verifying our rejection procedure. This procedure permitted an experiment whose efficiency for charge selection was nearly 100 percent. Our relative abundance results were therefore not dependent on understanding the pulse-height distributions in great detail.

Fragmentation within the apparatus is a source of systematic error which increases with charge. If fragmentation was violent enough to create extra prongs, one might expect that we could have rejected the event through detection of these prongs in the spark chambers. However, the spark robbing of nearby singly charged delta-rays showed that we probably see only the most heavily ionizing fragment leaving the interaction. Further, the most heavily ionizing fragment would be that portion of the parent nucleus which suffered the least momentum transfer and hence (provided the neutron/proton ratio was not greatly altered) would continue along the trajectory of the parent nucleus through our spectrometer. Therefore, fragmentation reactions in our apparatus would in fact not greatly affect the measurement of rigidity or the goodness of fit. We have made no attempt to reject or reclassify these events. Instead,

we have argued that fragmentations *above* our second scintillator would "feed down" like fragmentations in the overlying atmosphere, so we effectively took data at an increased atmospheric depth. Fragmentation *in* our second scintillator would be lost, since in this case the three scintillators would have greatly disparate pulse heights. Fragmentations *below* our second scintillator would not affect the charge assignment, since the first two scintillators would agree. Therefore, we have quoted an augmented residual atmosphere, and we have used a diminished apparatus attenuation. For our data, we feel this procedure has the least systematic error of the possible techniques to take account of fragmentation within the apparatus. However, we recognize in our procedure the weakness that fragmentations in the top half of our apparatus are not exactly like those far above us in the atmosphere, since the former are still accompanied by the various reaction products. Inevitably, there is no substitute for elimination of the residual atmosphere and minimization of the detector material.

The final source of systematic error we have discovered is the trigger discrimination threshold inefficiency for the lowest-$Z$ element with a particular threshold setting. Prior to flight we calibrated the equipment on sea-level muons, and these results carried directly over to protons in our $Z \geq 1$ trigger mode. Extrapolation to the $Z \geq 2$ mode was straightforward, and we checked it in our first flight by taking a portion of our $Z \geq 2$ data with a reduced threshold. For elements above helium, we calculate trigger threshold loss to be negligible; cross-checks within our data sets confirmed this calculation within our statistics.

In sum, we feel that our data agree well with other measurements, and that the disagreements of table 5 provide a measure of the true errors in the relative abundances. It looks as though systematic errors will be dominant in relative abundance measurements for some time to come. Even if the systematic errors in event recognition and background rejection were solved, we would still be severely limited in our astrophysical interpretation by uncertainties in the fragmentation parameters necessary for extrapolation to the top of the atmosphere and from there through the interstellar material back to the sources.

## VI. ABSOLUTE FLUXES

The relative abundances of table 3 are easily related to the absolute fluxes using the event data, the geometry factor, and the exposure times of table 2. At the top of our spark chambers we found a flux (events/m$^2$ sterad s) of 69.1 $\pm$ 2.6 for helium for the first flight, and of 84.1 $\pm$ 1.7 for the second flight. For carbon these fluxes were 1.71 $\pm$ 0.06 and 1.96 $\pm$ 0.04. Although our second flight took place an average of 1° further south in magnetic latitude than the first flight, and we observed a slightly larger geomagnetic cutoff, we had 15–20 percent higher fluxes for the second flight. Since the day before our second flight was a disturbed magnetic day (Lincoln 1971), this anomaly may be understandable. The Dallas neutron monitor (private communication with R. Palmeira) gave a 4 percent higher reading on the day of our second flight. To check the normalization between the two flights we considered only events whose rigidity was greater than 10 GV/$c$, and again compared fluxes. These high-rigidity fluxes agreed adequately within their errors. We are currently preparing a separate publication on analysis of the geomagnetic cutoffs, albedo, and solar-modulation effects observed in our flights. In any case, we feel there is no significant disagreement in absolute fluxes between the two flights. Correcting fluxes to the top of the atmosphere, we find helium fluxes (events/m$^2$ sterad s) of 82 $\pm$ 4 and 105 $\pm$ 3, and carbon fluxes of 2.18 $\pm$ 0.09 and 2.51 $\pm$ 0.06 for the respective flights, for their nominal geomagnetic cutoffs of 4.35 and 4.55 GV/$c$. Von Rosenvinge *et al.* quote fluxes for a 4.35 GV/$c$ cutoff of 91.5 $\pm$ 2 (1969*b*) for helium and of 2.63 $\pm$ 0.08 (1969*a*) for carbon.

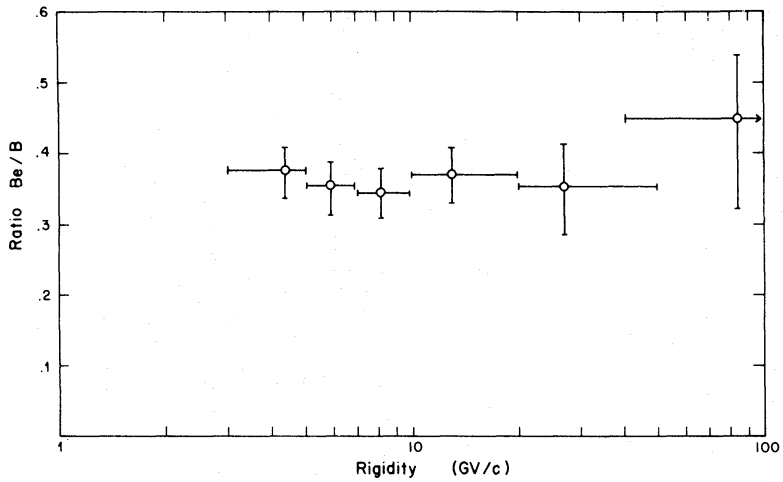


FIG. 3.—Ratio of beryllium to boron as a function of rigidity, uncorrected for $\sim 6.5$ g cm$^{-2}$ of equivalent overlying atmosphere.

## VII. BERYLLIUM/BORON RATIO VERSUS RIGIDITY

O'Dell *et al.* (1971) have calculated that the ratio Be/B should range from 0.29 at low rigidities, where $^{10}$Be presumably has decayed, to 0.42 at high rigidities, where $^{10}$Be presumably has not decayed. For cosmic-ray lifetimes of $\sim 10^6$ years, the bulk of this change occurs within the rigidity range covered by this experiment. For these ratios there is an uncertainty of $\pm 0.06$ in absolute scale. Figure 3 presents our measurements of the Be/B ratio as a function of rigidity. The average value of the ratio over the range of our data is $0.37 \pm 0.02$. This value drops to about $0.34 \pm 0.02$ when it has been corrected for atmospherically induced change using the calculated variation of Von Rosenvinge *et al.* (1969*a*). Our atmospheric corrections indicate a value of 0.28. Our value of the ratio is consistent within the errors of the calculation with *any* mean cosmic-ray lifetime within the errors of the presently permissible range of $10^6$ to $10^8$ years. The expected variation of the ratio with rigidity is too small to be discernible within our statistics. A definitive cosmic-ray age determination by this method will require greatly improved statistics.

## VIII. CARBON/OXYGEN, LIGHT/MEDIUM, AND OTHER RATIOS VERSUS RIGIDITY

Figure 4 shows the ratios He/C, H/He, O/C, and L/M (Li + Be + B)/(C + N + O) as a function of rigidity for our data. The H/He data come entirely from our first flight, since no proton events were recorded during the second flight. Examination of the other three ratios separately showed no significant difference between the two flights, so the data for both flights have been combined. We compensated proportionately, for L/M ratio, for the missing lithium data in $Z \geq 4$ blocks of Flight 2. No significant departure from constancy is seen as a function of rigidity for H/He, He/C, and O/C, although H/He may have a small slope. However, the L/M ratio changes significantly as a function of rigidity. Since more than 60 percent of the nitrogen we see is expected to be secondary in origin (Simpson 1971), we examined the nitrogen spectrum and found it to be similar to those of Li, Be, and B. Therefore, in figure 5 we present the ratio (Li + Be + B + N)/(C + O) as a function of rigidity. Elements with charge $Z \geq 8$ had spectra which were similar to that of (C + O). As in the previous section, we have presented our data *without* atmospheric correction.

Figure 5 shows that Li, Be, B, and N are characterized in our data by a diminishing abundance, relative to the other elements, as the rigidity increases. The decrease seems

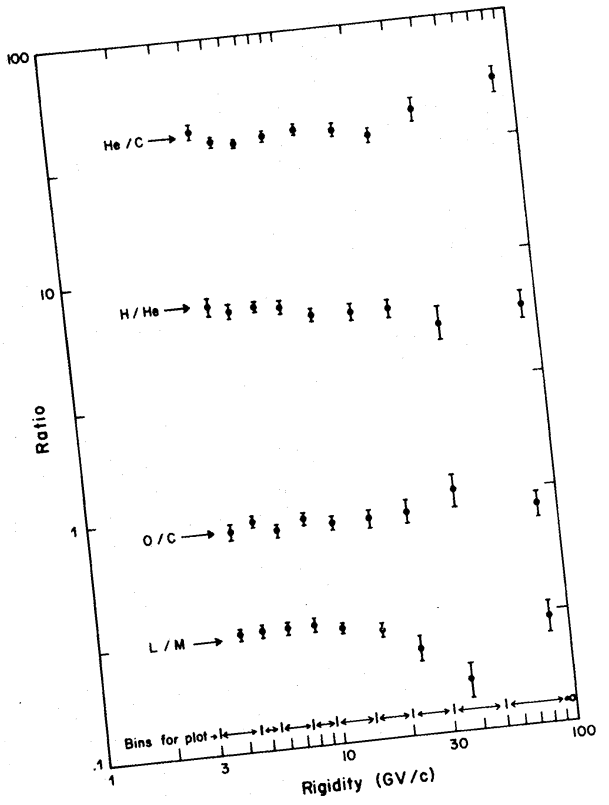


FIG. 4.—Various ratios as a function of rigidity, uncorrected for $\sim 6.5$ g cm$^{-2}$ of equivalent overlying atmosphere.

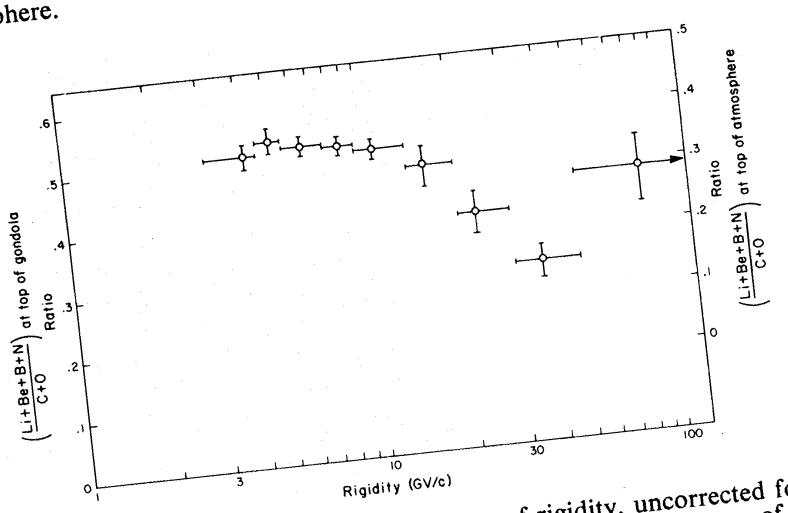


FIG. 5.—(Li + Be + B + N)/(C + O) as a function of rigidity, uncorrected for $\sim 6.5$ g cm$^{-2}$ of equivalent overlying atmosphere (*left-hand scale*) and corrected to the top of the atmosphere (*right-hand scale*).

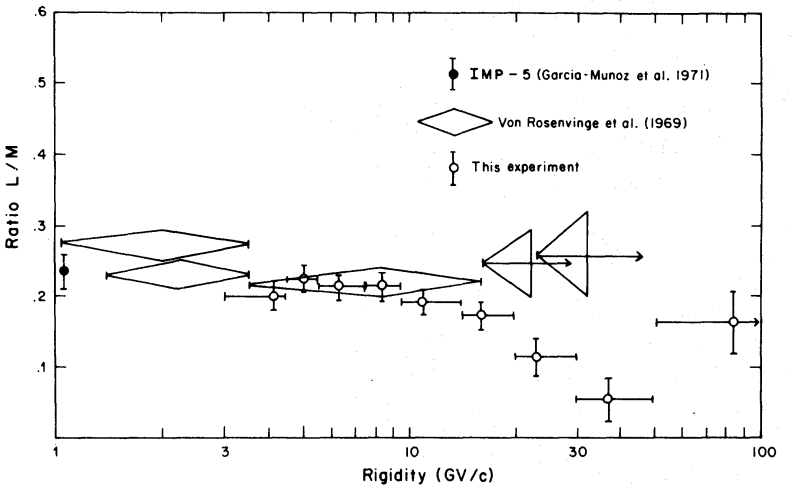


FIG. 6.—(L/M) ratio as a function of rigidity and corrected to the top of the atmosphere.

to begin at about 10 GV/$c$. The chance is less than $10^{-6}$ that the points above 10 GV/$c$ really had the same ratio as those below 10 GV/$c$, but suffered a statistical fluctuation to give the observed effect.

Viewed through the L/M ratio, our data agree well with lower-energy data. Using the fragmentation parameters and mean free paths of table 4 to correct the L/M ratio for the overlaying atmosphere (a reduction of 0.115 presumed to be rigidity-independent), we present in figure 6 our L/M ratio extrapolated to the top of the atmosphere. The data of Von Rosenvinge *et al.* (1969*a*) and an IMP-5 measurement (Garcia-Munoz, Mason, and Simpson 1971) are shown for comparison. The right-hand scale of figure 5 shows our (Li + Be + B + N)/(C + O) ratio similarly corrected to the top of the atmosphere.

We have examined our data analysis procedure to be sure that these diminishing relative abundances were not due to some instrumental effect. We have found no anomaly in our high rigidity events; the scanning topologies, goodness-of-fit, and charge distributions of these data all appear to be perfectly normal. As a final check, a selection of the highest rigidity events were hand-remeasured on our most accurate measuring machine. The new values of rigidity agreed with the old within expected errors.

## IX. RIGIDITY SPECTRA

The magnetic spectrometer measures rigidity in a most fundamental and direct way. Unlike other techniques, it does not depend on unaccountable corrections or calibrations. However, since this is the first magnetic spectrometer experiment with good statistics in this high-energy region, we feel it is appropriate here to explain in some detail how the rigidity spectra are extracted from the data.

The magnetic spectrometer measures the curvature of the charged particle trajectory. The deflection angle $\theta$ of an event has a fixed, Gaussian error distribution. The quantity $\theta$ is related to the rigidity $R$ by the relation

$$R = \frac{0.03\left|\int \boldsymbol{B} \times d\boldsymbol{l}\right|}{\theta}, \tag{1}$$

where the magnetic field integral, $\left|\int \boldsymbol{B} \times d\boldsymbol{l}\right|$, is in kilogauss-meters, $\theta$ is in radians, and $R$ is in (GV/$c$). For actual analysis it is much more convenient to analyze and fit

the data in terms of specific curvature $K \equiv 1/R$ because $K$ is directly proportional to the measured quantity $\theta$ and its value and error do not diverge as $\theta \to 0$. The average error in $K$ was roughly constant over the range of data in our apparatus, although individual-event error assignments varied by a factor of $2\frac{1}{2}$ because $|\int \boldsymbol{B} \times d\boldsymbol{l}|$ was different for each event.

Random errors had contributions from film measurement error, from small-scale uncertainties in the optical calibrations, and from spatial spark jitter. These errors in specific curvature were studied by spark-fitting within a chamber, by consistency cross-checks in the optical calibrations, and finally by detailed analysis and fitting of the undeflected "straight-track" events taken for each flight with the magnet off. The spark jitter was found to be about $\pm 0.2$ mm per spark for protons. Sparks produced by higher charged incident particles had proportionally less jitter, as expected with the increased ionization energy deposited in the spark chamber gaps (Smoot *et al.* 1972*a*). Measurement error from SASS was about $\pm 0.2$ mm per four-spark average, and the optics error was $\pm 0.14$ mm per four-spark average. For complex nuclei these errors combined to yield a mean error in specific curvature of $\pm 0.020$ $c$/GV for the first flight and $\pm 0.018$ $c$/GV for the second. These values correspond to a mean maximum resolvable rigidity of 50 GV/$c$ for the first flight and 55 GV/$c$ for the second flight.[2] Because of the added contribution from spark jitter, the proton resolution was approximately 10 percent poorer than the above.

Commonly one fits the rigidity (or energy) spectra to a power law of the form

$$dN/dR = N_0 R^{-\gamma}, \tag{2}$$

where $\gamma$ is the "spectral index" and $N_0$ is a normalization constant. In terms of $K$ the function is

$$dN/dK = N_0 K^{\gamma-2}. \tag{3}$$

TABLE 6

RESULTS OF RIGIDITY-SPECTRA FITTING
(Spectra have been fit to $dN/dR = N_0 R^{-\gamma}$ above 8.3 GV/$c$)

| Charge Group ($Z$) | $\gamma$ | $\chi^2$ of the Fit (for 50 degrees of freedom) | Integral Flux above 8.3 GV/$c$ |
|---|---|---|---|
| 1 | 2.63 ± 0.08 | 41 | 175 |
| 2 | 2.47 ± 0.03 | 81 | 33 |
| 3 | 2.67 ± 0.13 | 68 | 0.18 |
| 4 | 2.66 ± 0.12 | 52 | 0.09 |
| 5 | 2.76 ± 0.08 | 48 | 0.22 |
| 6 | 2.54 ± 0.04 | 46 | 0.81 |
| 7 | 2.72 ± 0.09 | 37 | 0.21 |
| 8 | 2.52 ± 0.05 | 69 | 0.71 |
| 9–14 | 2.52 ± 0.07 | 55 | 0.58 |
| 6 + 8 | 2.53 ± 0.03 | 70 | 1.52 |
| 3 + 4 + 5 + 7 | 2.72 ± 0.05 | 40 | 0.70 |

* Spectra are below $\sim 6.5$ g cm$^{-2}$ of residual atmosphere; flux units are (particles per m$^2$ per sterad per second).

[2] The higher value of rigidity resolution quoted for the antimatter search with this instrument (Buffington *et al.* 1972) was achieved with a more accurate measuring machine than SASS. Unfortunately, this hand-operated machine was too slow to be practical for measuring the large amounts of data presented here.

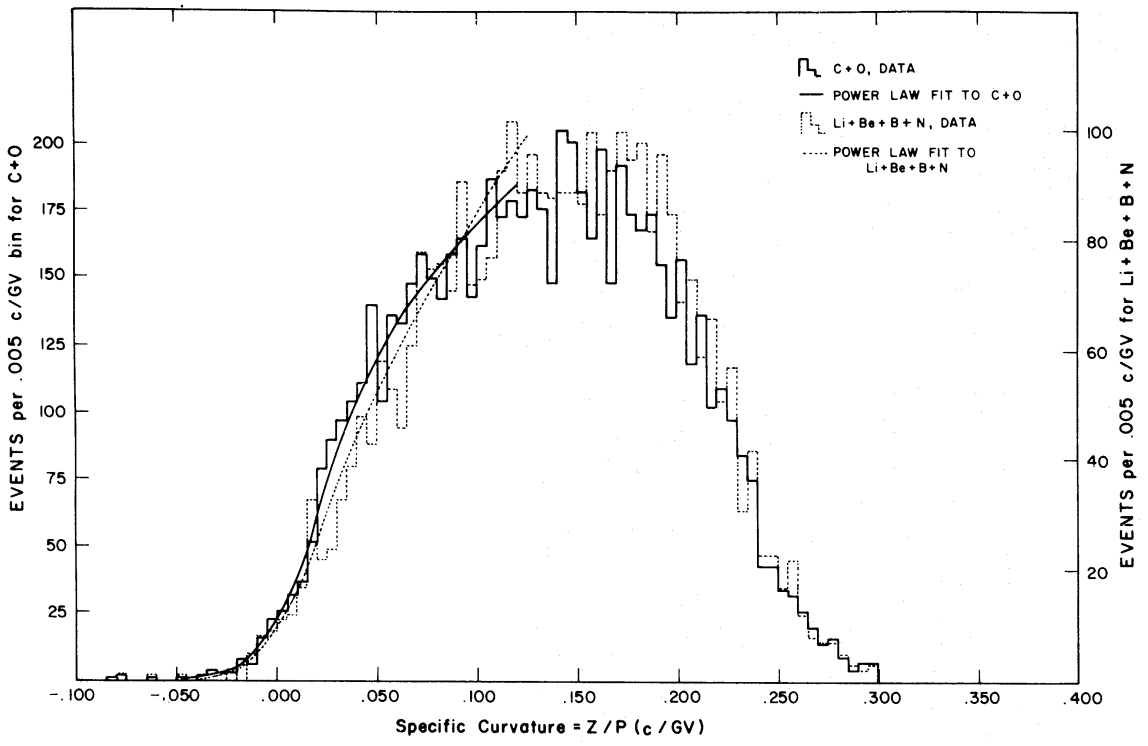


FIG. 7.—Specific curvature distributions for (Li + Be + B + N) and for (C + O), uncorrected for $\sim 6.5$ g cm$^{-2}$ for overlying atmosphere. The histograms are normalized to the same area.

We used a maximum-likelihood technique (Eberhard and Koellner 1970) to select the best values of $N_0$ and $\gamma$ for fitting each data set. By varying the maximum specific curvature (minimum rigidity) considered for the fit, we found that geomagnetic effects were greatly reduced for $K \leq 0.12$. Solar modulation was neglected in our fitting procedure.

Table 6 presents the spectral indices and $\chi^2$ of the fit for our various data sets. For the anti-IN data, the charge and rigidity-dependent delta-ray bias was removed by an appropriate weighting of events. The fitting procedure was checked using Monte Carlo generated events. The Monte Carlo runs also verified the error assignments for statistical fluctuations in the data. Table 6 also presents integral fluxes above an artificial cutoff at 8.3 GV/$c$. The increasing scarcity of (Li + Be + B + N) with increasing rigidity now manifests itself as a spectral index which is $0.19 \pm 0.06$ larger than that for (C + O).[3] The statistical significance of this result is less than the significance of change in the ratio (Li + Be + B + N)/(C + O) in figure 5 because the data below 8.3 GV/$c$ were ignored in fitting the rigidity spectra.

The statistical significance of our changing ratio shows most clearly when we compare directly the specific curvature histograms for the two data groups, (Li + Be + B + N) and (C + O). This is done in figure 7. Actual numbers of events were added together with no correction for the delta-ray losses incurred in the anti-IN portion of the data. Geomagnetic cutoff limits the data at $K \geq 0.25$ $c$/GV. As in the previous section, it is apparent from figure 7, as $K$ approaches zero from its peak

[3] *Note added in proof.*—This is the effect which we reported at the San Juan Conference, 1971 December, stating that "the combined spectral index for elements Li, Be, B, and N was found to be steeper than that for C + O by $\Delta\gamma = 0.12 \pm 0.04$." Our present value is the result of a careful fit, using all our data. We note that our observations of steeper spectra have now been confirmed by another group (E. Juliusson *et al.*, *Phys. Rev. Letters*, **29**, 445 [1972]).

1973ApJ...180..987S

## TABLE 7

MEASURED DIFFERENTIAL FLUXES OF THE ELEMENTS
(Particles/m² ster sec GV/*c*)
(*not* corrected for ~6.5 g cm⁻² of overlaying atmosphere)

| Charge Group | MEAN RIGIDITY* 5.0 | 6.3 | 8.4 | 11.3 | 16.4 | 23.7 | 37 | 65 | 156 |
|---|---|---|---|---|---|---|---|---|---|
| 1†..... | 72 ± 4 | 57 ± 3 | 34 ± 2 | 14.8 ± 0.9 | 5.7 ±0.4 | 2.2 ±0.2 | 0.67 ±0.10 | 0.13 ±0.03 | 0.015 ±0.004 |
| 2†..... | 11.0 ± 0.2 | 9.2 ±0.2 | 5.7 ±0.1 | 2.71 ±0.08 | 1.05 ±0.04 | 0.40 ±0.02 | 0.144 ±0.010 | 0.028 ±0.002 | 0.0034 ±0.0005 |
| 3..... | 0.070 ±0.008 | 0.067 ±0.005 | 0.037 ±0.004 | 0.017 ±0.002 | 0.0061 ±0.0010 | 0.0024 ±0.0005 | 0.00034 ±0.00013 | 0.00020 ±0.00006 | 0.000011 ±0.000007 |
| 4..... | 0.040 ±0.004 | 0.031 ±0.003 | 0.018 ±0.002 | 0.008 ±0.001 | 0.0031 ±0.0005 | 0.0009 ±0.0003 | 0.00022 ±0.00007 | 0.00006 ±0.00002 | 0.000007 ±0.000004 |
| 5..... | 0.121 ±0.008 | 0.086 ±0.004 | 0.057 ±0.003 | 0.022 ±0.002 | 0.0081 ±0.0009 | 0.0026 ±0.0003 | 0.00075 ±0.00014 | 0.00028 ±0.00006 | 0.000012 ±0.000005 |
| 6..... | 0.302 ±0.012 | 0.261 ±0.008 | 0.153 ±0.007 | 0.072 ±0.003 | 0.0286 ±0.0014 | 0.0118 ±0.0008 | 0.0035 ±0.0003 | 0.00066 ±0.00009 | 0.000069 ±0.000014 |
| 7..... | 0.100 ±0.007 | 0.076 ±0.004 | 0.045 ±0.003 | 0.021 ±0.002 | 0.0073 ±0.0008 | 0.0028 ±0.0004 | 0.00083 ±0.00017 | 0.00018 ±0.00004 | 0.000010 ±0.000005 |
| 8..... | 0.267 ±0.012 | 0.198 ±0.008 | 0.130 ±0.006 | 0.056 ±0.003 | 0.0230 ±0.0016 | 0.0101 ±0.0009 | 0.0034 ±0.0003 | 0.00050 ±0.00008 | 0.000049 ±0.000012 |
| 9–14..... | 0.194 ±0.014 | 0.156 ±0.009 | 0.097 ±0.003 | 0.048 ±0.003 | 0.0227 ±0.0021 | 0.0083 ±0.0009 | 0.0021 ±0.0003 | 0.00043 ±0.00010 | 0.000078 ±0.000020 |
| 15–23..... | 0.049 ±0.008 | 0.034 ±0.005 | 0.018 ±0.004 | 0.011 ±0.002 | 0.0043 ±0.0009 | 0.0019 ±0.0005 | 0.0008 ±0.0003 | 0.00015 ±0.00007 | 0.000029 ±0.000012 |
| ≥24..... | 0.030 ±0.006 | 0.020 ±0.004 | 0.018 ±0.004 | 0.006 ±0.001 | 0.0023 ±0.0007 | 0.0010 ±0.0004 | 0.0004 ±0.0002 | 0.00012 ±0.00006 | 0.000015 ±0.000010 |

* Bin edges for these differential flux evaluations were at the following values of rigidity: 4.5, 5.5, 7.5, 9.5, 14, 20, 30, 50, and 100 GV/*c*.

† In addition to the statistical errors shown here, there is an overall flux uncertainty of 10 percent for hydrogen and 5 percent for helium, due to uncertainty in trigger threshold determinations.

value at $\approx 0.13\ c$/GV, that (lithium + beryllium + boron + nitrogen) becomes increasingly rare relative to (carbon + oxygen). The smooth curves in figure 7 are the results of the fitting procedure described above. Examination of the specific curvature plots for protons, for helium, and for the elements with charge greater than oxygen showed each to be similar to that of (carbon + oxygen).

Table 7 presents our measured differential spectra, uncorrected for the overlaying atmosphere. The differential spectra for H, He, and C are corrected for the overlaying atmosphere and plotted in figure 8. The fluxes are in reasonable agreement with the recently published measurements of the Goddard calorimeter group (Ryan, Ormes, and Balasubrahmanyan 1972), with the measurements of Anand *et al.* (1968), and with Von Rosenvinge *et al.* (1969*a*, *b*). Our data below $\sim 8$ GV/$c$ are low compared with the other data, due to the effect of geomagnetic cutoff in our flights.

Since the group (phosphorus through chromium) probably has a similar origin to (Li + Be + B + N), we might expect similar spectral indices for these two groups. Unfortunately within the statistics of this experiment it is not possible to tell whether this is so.

In the case of (Li + Be + B + N), correction of the spectral index to the top of the atmosphere will yield a different value. Assuming that 26 percent of (Li + Be + B + N) was due to (C + O) fragmentation and that each daughter nucleus had the parent's spectral index, we find that the difference in spectral index between (Li + Be + B + N) and (C + O) becomes $0.31 \pm 0.10$ at the top of the atmosphere.

## X. DISCUSSION

Both figure 5 and our fitted values for spectral indices indicate that the elements lithium, beryllium, boron, and nitrogen become increasingly rare relative to the other elements as rigidity increases from 10 to 100 GV/$c$. We have been unable to discover any systematic source of error in our equipment or analysis procedure which could produce this effect. The chance that it is a statistical fluctuation is small. We are currently preparing for the flight of a new instrument which has greatly simplified optics and calibration procedures relative to the instrument whose measurements are presented here. We expect this new instrument to reduce the errors of the spectral indices to a level where the difference in index observed here (above 8 GV/$c$) should be a $4\frac{1}{2}$ standard deviation effect.

An explanation of our observations would be provided if there were a variation with rigidity of the cross-section for fragmentation reactions. Direct measurements of some of the fragmentation cross-sections, using protons incident on heavy targets and a mass spectrograph to measure the products, have shown them to remain constant within about 10 percent over our rigidity range (Shapiro and Silberberg 1970; Silberberg and Tsao). To explain our measurement, the cross-sections would have to diminish by 30–40 percent as the rigidity increases from 10 to 100 GV/$c$. However, the bulk of the important fragmentation reactions have not been definitively measured over our rigidity range, so variation of cross-section cannot be excluded as an explanation, although at this time it seems unlikely.

An intriguing alternative explanation would be provided by a variation of cosmic-ray material traversed as a function of rigidity. We sketched, in § I, the reasons for believing that material traversed and hence the "lifetime" should be constant within our rigidity range. But the power-law dependence of the total cosmic-ray energy spectrum may be the result of a more complicated containment situation than that currently envisaged. If so, our observation would be most easily and naturally accommodated by a cosmic-ray material traversal whose magnitude diminishes as the rigidity increases over our range. Variation in material traversal would be, in turn,

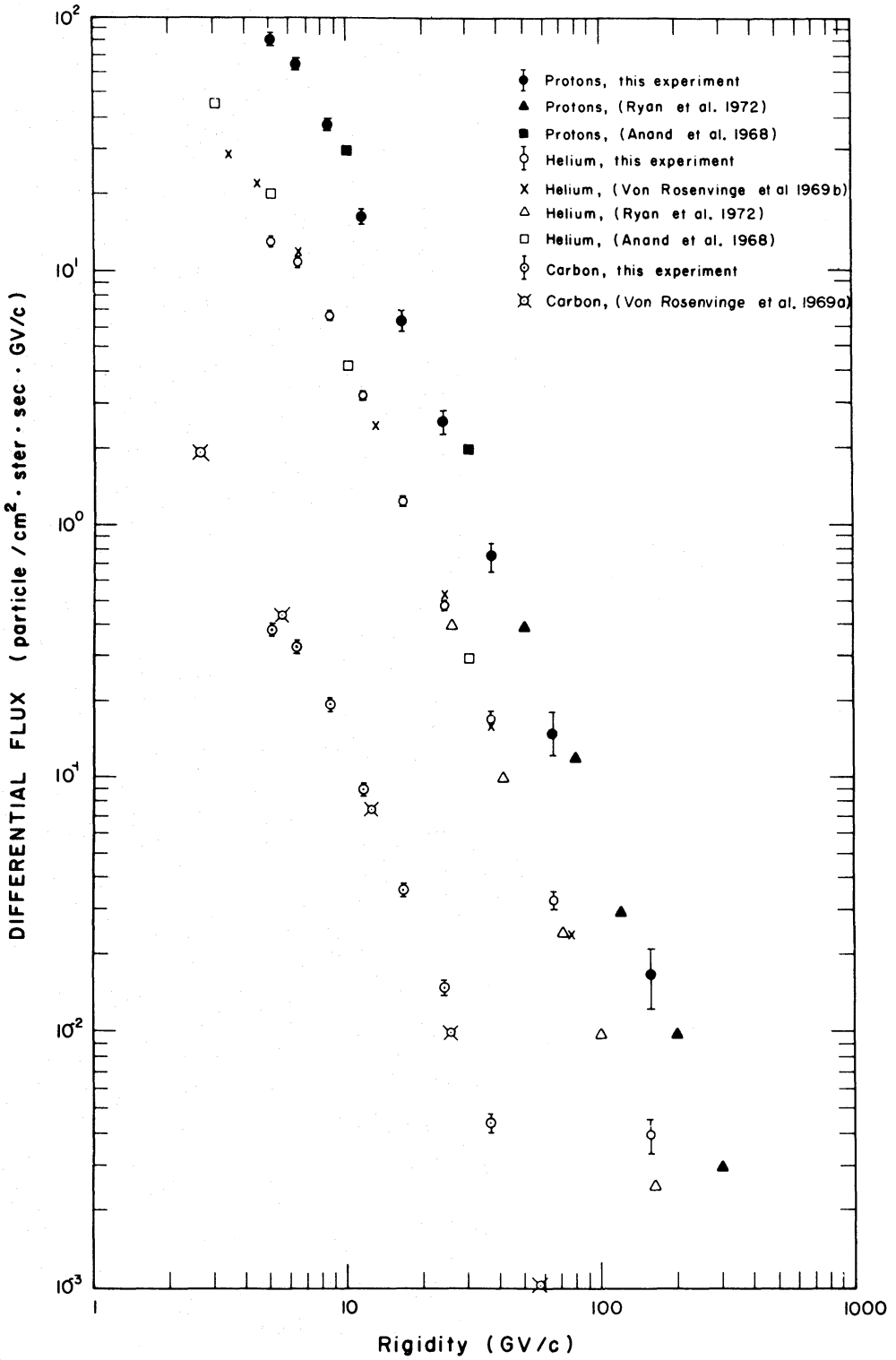


FIG. 8.—Rigidity distribution measurements of protons, helium, and carbon, corrected to the top of the atmosphere.

most easily accommodated by an equivalent variation in the cosmic-ray mean lifetime itself.

The design, construction, test, and flight of this instrument, and the subsequent data analysis, represent a continued and tenacious effort over the course of several years, for many more individuals than those listed as authors on this paper. Particular note should be made of Ben Clawson, who oversaw many of our mechanical details, and of Joe Orsini, who was in charge of our electronics. Gladys Sessler did much of the programming and library work in the data analysis. We also give thanks to our excellent crew of scanners and to the personnel at the Lawrence Berkeley Laboratory technical photography division. Our flights took place from the NSF-supported National Center for Atmospheric Research launch facility at Palestine, Texas. We would like to thank the Palestine launch crew for the kind hospitality extended to us during our operations there and to thank Dr. M. Schwarzschild for use of the Stratoport building. In interpretation and correction of the data we would like to acknowledge stimulating and useful conversations with Drs. R. Silberberg, M. Shapiro, C. J. Waddington, R. Cowsik, and R. Muller. Drs. P. Dauber and C. Orth helped with the critical reading of the manuscript. Finally we want to thank the many individuals within the National Aeronautics and Space Administration, particularly Drs. John Naugle, Harvey Hall, and Albert Opp, who have encouraged and supported us in this work.

## REFERENCES

Anand, K. C., Daniel, R. R., Stephens, S. A., Bhowmik, B., Krishna, C. S., Aditya, P. K., and Puri, R. K. 1968, *Canadian J. Phys.*, **46**, S652.
Buffington, A., Smith, L. H., Smoot, G. F., Wahlig, M. A., and Alvarez, L. W. 1971, Paper OG-45, Twelfth International Conference on Cosmic Rays, Hobart, Tasmania, Australia, 1971, Conference Proceedings, **1**, 147.
Buffington, A., Smith, L. H., Smoot, G. F., Alvarez, L. W., and Wahlig, M. A. 1972, *Nature*, **236**, 335.
Cassé, M., Corydon-Peterson, O., Dayton, B., Koch, L., Lund, N., Melgaard, K., Mestreau, P., Meyer, J. P., Omø, K., Risbo, T., and Roussel, D. 1971*a*, Proc. Cospar Conference, Leningrad, Space Research XI.
Cassé, M., Koch, L., Lund, N., Meyer, J. P., Peters, B., Soutoul, A., and Tandon, S. N. 1971*b*, Paper OG-68, Twelfth International Conference on Cosmic Rays, Hobart, Tasmania, Australia, 1971, Conference Proceedings, **1**, 241.
Clayton, D. D. 1968, *Principles of Stellar Evolution and Nuclear Synthesis* (New York: McGraw-Hill).
Cleghorn, T. F., Freier, P. S., and Waddington, C. J. 1968, *Canadian J. Phys.*, **46**, S572.
Colgate, S., and White, R. H. 1966, *Ap. J.*, **143**, 626.
Comstock, G. M. 1969, *Ap. J.*, **155**, 619.
Cowsik, R. 1970, *Ap. Letters*, **6**, 39.
Eberhard, P. H., and Koellner, W. O. 1970, UCRL 20159, October.
Garcia-Munoz, M., Mason, G. M., and Simpson, J. A. 1971, Paper OG-62, Twelfth International Conference on Cosmic Rays, Hobart, Tasmania, Australia, Conference Proceedings **1**, 209.
Gloeckler, G., and Jokipii, J. R. 1970, *Acta Physica Academiae Scientiarum Hungaricae*, **29**, Suppl. 1, 541.
Gold, T. 1968, *Nature*, **218**, 731.
Goldreich, Peter, and Keeley, D. A. 1969, "Near Field Acceleration in Pulsars," Rome Conference on Pulsars, December.
Hayakawa, Satio. 1969, *Cosmic Ray Physics*, Volume **22**, p. 534 (New York: Interscience).
Jokipii, J. R., and Parker, E. N. 1969, *Ap. J.*, **155**, 799.
Kulsrud, R. M., Ostriker, J. P., and Gunn, J. E. 1971, preprint PPL-AP49, Plasma Physics Laboratory, Princeton University, October.
Lincoln, J. V. 1971, *J. Geophys. Res.*, **76**, 6212.
Lingenfelter, R. E. 1969, *Nature*, **224**, 1182.
O'Dell, F. W., Shapiro, M. M., Silberberg, R., and Tsao, C. H. 1971, Paper OG-59, Twelfth International Conference on Cosmic Rays, Hobart, Tasmania, Australia, 1971, Conference Proceedings, **1**, 197.
Ostriker, J. P., and Gunn, J. E. 1969, *Ap. J.*, **157**, 1395.

Ryan, M. J., Ormes, J. F., and Balasubrahmanyan, V. K. 1972, *Phys. Rev. Letters*, **28**, 985.
Shapiro, M. M., and Silberberg, R. 1970, *Ann. Rev. Nucl. Sci.*, **20**, 323–392.
Shivanandan, K., Houck, J. R., and Harwit, M. 1968, *Phys. Rev. Letters*, **21**, 1460.
Silberberg, R., and Tsao, C. H., "Partial Cross Sections in High-Energy Nuclear Reactions for Targets with $Z \leq 28$," Naval Research Laboratory, Washington, D.C. 1971.
Simpson, J. A. 1971, Rapporteur paper, Twelfth International Conference on Cosmic Rays, Hobart, Tasmania, Australia, 1971 (Enrico Fermi Institute Laboratory for Astrophysics and Space Research, preprint #71–73).
Smith, L. H., Buffington, A., Wahlig, M. A., and Dauber, P. 1972, *Rev. Sci. Instr.*, **43**, 1.
Smoot, G. F., Buffington, A., and Smith, L. H. 1972*a*, *Rev. Sci. Instr.*, **43**, 1285.
Smoot, G. F., Buffington, A., Smith, L. H., Alvarez, L. W., and Wahlig, M. A. 1972*b*, Proc. of the Joint Meeting of the APS and AAS, San Juan, Puerto Rico, December, 1971, reported in *IKK, Zentrastelle fur Atomickernenergie*, Number 3.
Speller, R., Thambyahpillai, T., and Elliot, H. 1972, *Nature*, **235**, 25.
Von Rosenvinge, T. T., Webber, W. R., and Ormes, J. F. 1969*a*, *Ap. and Space Sci.*, **3**, 4–13 and 80–101.
———. 1969*b*, *ibid.*, **5**, 342–369.
Webber, W. R., Damle, S. V., and Kish, J. M. 1972, *Ap. and Space Sci.*, **15**, 245.
Zurlinden, Donald H. 1970, SASS (Spark Chamber Automatic Scanning System), Report No. UCRL-17695, Lawrence Radiation Laboratory, Berkeley, University of California, 1967; Datamation, March, 1970.